THEORY OF THE METEOR HEIGHT DISTRIBUTION OBTAINED FROM RADIO-ECHO OBSERVATIONS

I. Shower Meteors

T. R. Kaiser

(Communicated by A. C. B. Lovell)

(Received 1953 August 21)

Summary

Apart from a slight influence of the directional properties of the aerial system, the form of the radio-echo height distribution for a homogeneous velocity group of meteors constituting a stream with a well-defined radiant point is found to be a function only of the atmospheric scale height and the mass distribution of the incident meteors. The relation between these parameters and the width of the height distribution (expressed as the r.m.s. deviation from the mean) is derived, hence if one is known the other may be determined from the observed meteor heights. The mean height corresponds to a value of the atmospheric pressure which is related to the physical properties of the meteors, their ionizing efficiency and velocity, and the radio-echo equipment parameters. The theory enables the observed dependence of the mean height on the velocity to be interpreted in terms of the variation of atmospheric pressure with height.

1. *Introduction.*—The passage of a meteor through the atmosphere produces a column of ionization which may be detected by the scattering of radio waves from it. In the absence of distortion of the linear trail (by winds, etc.) the reflection is specular, i.e. the important part of the trail is a length of the order of $\sqrt{(R\lambda)}$ (R = range, λ = wave-length) centred about the normal intersection of a radius vector from the observing station with the trail. We will call this the reflection point. The characteristics of the observed radio echo are dependent primarily upon the electron line density in the trail and on the properties of the atmosphere in the vicinity of the reflection point (**1, 2**).

Clegg and Davidson (**3**) have described an apparatus for determining the elevation and range, and hence the height of the reflection points. The purpose of this paper is to develop a theory of the dependence of the observed height distribution on the properties of the incident meteors and of the atmosphere in the meteor ionization region, and on the parameters of the radio equipment. The discussion is restricted here to a homogeneous velocity group of meteors constituting a stream with a well-defined radiant point.

2. *Theory of meteor ionization.*—In passing through the upper atmosphere, a meteor is subject to individual collisions with air molecules, a great proportion of which are trapped in its surface. The heat liberated causes the meteor to evaporate atoms which leave with thermal velocities relative to the meteor surface but carry the meteor velocity relative to the surrounding atmosphere. Subsequent collisions between meteor atoms and air molecules produce ionization and excitation, mainly of the meteor atoms (**4**).

Herlofson (**5**) and Whipple (**6**) have summarized the modern theory of the motion of a meteoric particle in a rarefied atmosphere, from which we obtain the following expression for the rate of evaporation:

$$n=(\mu H)^{-1}mv\cos\chi\,(p/p_{\max})[1-\tfrac{1}{3}(p/p_{\max})]^2; \qquad (1)$$

$p_{\max}$ is the atmospheric pressure at the point of maximum rate of evaporation and is given by

$$p_{\max}=[(2lg)/(\Lambda v^2 A)]m^{1/3}\cos\chi, \qquad (2)$$

where $A=\mathscr{A}m^{-2/3}$, $\mathscr{A}$ is the initial cross-sectional area of the meteor in its line of flight in cm^2 and m is its initial mass in g. It should be noted that A, which Whipple calls the " shape factor ", is independent of m, being a function only of the shape of the meteor and of its density. The other quantities appearing in (1) and (2) are as follows:

n (sec^{-1}) = number of meteor atoms evaporated per second,
v (cm sec^{-1}) = meteor velocity,
μ (g) = mass of an individual meteor atom,
l (erg g^{-1}) = latent heat of evaporation of the meteor,
χ = zenith angle of the meteor radiant,
p (dyne cm^{-2}) = atmospheric pressure,
H (cm) = atmospheric scale height,
g (cm sec^{-2}) = gravitational acceleration,
Λ = heat transfer coefficient.

The heat transfer coefficient (**6**) is defined as the ratio (heat energy liberated)/(air mass intercepted by the meteor $\times\,\frac{1}{2}v^2$). Herlofson takes $\Lambda=1$, i.e. he assumes that all impinging air molecules are trapped in the meteor surface, while Whipple suggests a value of about 0·7.

In deriving (1) and (2) the deceleration of the meteor is assumed to be small, and approximations have been made which require $v^2\gg 12l$. The error at small velocities mainly affects equation (2). The zenith angle is assumed to be constant along the length of the trail, i.e. $(90^\circ-\chi)$ must be at least several degrees.

The electron line density produced by the meteor is $\alpha=\beta n/v$, where β is the probability that a single evaporated meteor atom will give rise to a free electron; β may be a function of v.

We will restrict ourselves to the case of a meteor shower, comprising a homogeneous velocity group of meteors with a well-defined radiant. Writing

$$k_1=\beta/(\mu H), \quad k_2=2lg/(\Lambda v^2 A)$$

we find that α electrons per cm are produced, at pressure p, by a meteor of mass

$$m=\left[\left(\frac{k_2\alpha}{k_1 p}\right)^{1/2}+\frac{p}{3k_2\cos\chi}\right]^3. \qquad (3)$$

3. *The meteor mass distribution.*—Since $p_{\max}$ is a function of the meteor mass, the height distribution will depend upon the mass distribution of the incident meteors.

From a statistical analysis of visual observations Watson (**7**, **8**) and Williams (**9**) have shown that, over a wide range of visual magnitudes, the frequency increases by a constant ratio, a, per magnitude. This leads to the mass frequency law

$$\nu_M=bm^{-s}, \qquad (4)$$

where $\nu_M dm$ is the number of meteors in the mass group $m-(m+dm)$, crossing unit area normal to the stream per second, b is a constant and

$$s=1+2{\cdot}5\log_{10}a. \tag{5}$$

The above authors give values of a between 2 and 4, hence we may expect s to be in the vicinity of 2.

4. *Radio-echo height distribution.*—In the main part of this discussion we shall assume that the sensitivity of the apparatus is such that the majority of the meteor trails detected have electron line densities less than $10^{12}\,\mathrm{cm}^{-1}$ (short-duration echoes) and take the echo amplitude as directly proportional to α. The case where all echoes are from trails of line density greater than $10^{12}\,\mathrm{cm}^{-1}$ will be dealt with in Section 4.5 below.*

On account of the specular reflection from the trails, all of the echoing points lie in a plane ABCD (Fig. 1) passing through the observing station, O, normal to the radiant direction. The constant height (and pressure) contours are slightly curved lines, SS′, in this plane.

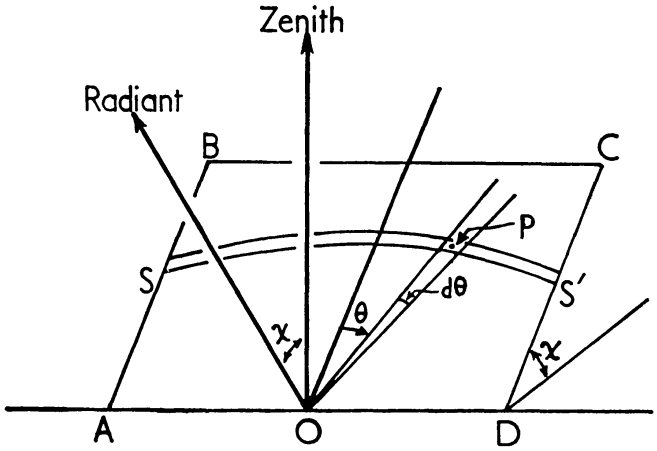

FIG. 1.—*The echo plane ABCD is normal to the radiant direction and is at elevation χ above the horizontal. $\pi/2-\theta$ is the angle in the echo plane, measured from the horizontal.*

4.1. *Height distribution from echoes obtained in the sector $\theta-(\theta+d\theta)$.*—Consider the point P, at height h, in the sector $\theta-(\theta+d\theta)$ of the echo plane (Fig. 1). The minimum electron line density detectable at P is given by

$$\alpha_P=KR^{3/2}S^{-2}(\theta), \tag{6}$$

subject to $\alpha_P<10^{12}$. $S(\theta)$ represents the aerial polar diagram (amplitude) in the echo plane, $R(\mathrm{cm})=\mathrm{OP}$, and K is a constant determined by the equipment parameters. It is given (1) by

$$K=6{\cdot}3\times10^{13}(\eta G_m)^{-1}[\epsilon/(P\lambda^3)]^{1/2}, \tag{7}$$

where G_m = aerial power gain (referred to an isotropic radiator) in the direction of the maximum of the beam in the echo plane,

$\lambda(\mathrm{cm})$ = wave-length,

P = peak transmitter power,

ϵ = minimum detectable echo power,

η is a constant which depends on the orientation of the incident electric field vector to the meteor trail. Its value lies between 1·0 for parallel polarization and 2·0 for transverse polarization.

* For a discussion of the variation of echo amplitude and duration with electron line density, see Kaiser and Closs (1); Closs, Clegg and Kaiser (2); and Greenhow (10).

From (3), writing

$$z=(p/k_2)\,[9\alpha_P\cos^2\chi/(4k_1)]^{-1/3}, \tag{8}$$

we find that the smallest detectable meteor passing through P has a mass

$$m_P=\frac{\alpha_P}{12k_1\cos\chi}\,(2z^{-1/2}+z)^3. \tag{9}$$

The number of detectable meteors passing per second through unit area at P is obtained by integrating the right-hand side of (4) with respect to m, between limits m_P and infinity. Thus the rate at which meteors will be observed in the sector $\theta-(\theta+d\theta)$, and within the height range $h-(h+dh)$, is $\nu_1\,d\theta\,dh$, where

$$\nu_1=\frac{b}{(s-1)}\left(\frac{12k_1\cos\chi}{\alpha_P}\right)^{s-1}\frac{R}{(R/R_e+\cos\theta\sin\chi)}\,\frac{1}{(2z^{-1/2}+z)^{3(s-1)}}. \tag{10}$$

R_e is the Earth's radius.

Except for α_P in (8), z varies directly as the pressure. When $z=1$, let $\alpha_P=\alpha_1$, $p=p_1$, $R=R_1$, $h=h_1$. Then

$$z=(p/p_1)\,(\alpha_1/\alpha_P)^{1/3}=(p/p_1)\,(R_1/R)^{1/2}.$$

Now R cannot vary more rapidly than directly as h, so putting $R_1/R=h_1/h$ we get

$$z=\frac{p}{p_1}\left(1-\frac{H}{2h_1}\ln\frac{p}{p_1}\right),$$

where

$$p_1=k_2\,[9\alpha_1\cos^2\chi/(4k_1)]^{1/3}. \tag{11}$$

Since meteor echoes are observed only over a few scale heights, with a mean height in the vicinity of 100 km, we can put $z=p/p_1$. For the same reason we find that the only significant height-dependent term in (10) is that containing z and, although R is a function of height, negligible error is involved in putting $R=R_1$ throughout. The normalized height distribution for echoes observed in the sector $\theta-(\theta+d\theta)$ is thus

$$\nu_1{}^*=\left(\frac{3}{2z^{-1/2}+z}\right)^{3(s-1)} \tag{12}$$

and

$$\nu_1\simeq\frac{b}{(s-1)}\left(\frac{4k_1\cos\chi}{9\alpha_1}\right)^{s-1}\frac{R_1}{(R_1/R_e+\cos\theta\sin\chi)}\,\nu_1{}^*, \tag{13}$$

subject to the restriction that χ does not approach 90°.

In most cases $\cos\theta\sin\chi\gg R_1/R_e$ and

$$\nu_1\simeq\frac{b}{(s-1)}\left(\frac{4k_1\cos\chi}{9\alpha_1}\right)^{s-1}\frac{h_1}{\cos^2\theta\sin^2\chi}\,\nu_1{}^*. \tag{14}$$

4.2. *Properties of the height distribution* $\nu_1{}^*$.—Putting $x_1=-\ln z$ we have

$$\nu_1{}^*=\left(\frac{3e^{x_1}}{2e^{3x_1/2}+1}\right)^{3(s-1)}, \tag{15}$$

where, for constant scale height,

$$x_1=(h-h_1)/H. \tag{16}$$

Fig. 2 gives $\nu_1{}^*$ as a function of x_1 for a range of values of s. The most probable height occurs at $x=0$, i.e. at height h_1, pressure p_1, and is independent of s. It is easily shown that α_1, the minimum line density detectable at range $R_1=h_1/(\cos\theta\sin\chi)$, is that produced by the meteor which has a maximum rate of

evaporation at pressure p_1. The width of the height distribution is a function only of s and of the scale height.

Due to the slight asymmetry of the height distribution, the mean value of x_1 is not zero. Denoting it by $\bar{x}_1$ we have

$$\bar{x}_1=(\bar{h}-h_1)/H=\frac{\int_{-\infty}^{\infty} x_1 v_1^* \, dx_1}{\int_{-\infty}^{\infty} v_1^* \, dx_1}. \tag{17}$$

The r.m.s. deviation of x_1 from the mean value we will denote by δx_1. Thus

$$(\delta x_1)^2=\frac{\int_{-\infty}^{\infty} (x_1-\bar{x}_1)^2 v_1^* dx_1}{\int_{-\infty}^{\infty} v_1^* \, dx_1}. \tag{18}$$

Both $\bar{x}_1$ and δx_1 are independent of θ, being functions only of s. They have been determined by numerical integration and are given in Fig. 3.

The integral of v_1^* with respect to x_1 will be of interest for later work concerned with the total meteor echo rate. To a good approximation it is given by

$$\int_{-\infty}^{\infty} v_1^* \, dx_1=2{\cdot}3\,(s-1{\cdot}13)^{-1/2}, \tag{19}$$

which is accurate to better than 1 per cent for $s>\frac{4}{3}$.

4.3. *Complete height distribution, polar diagram symmetrical about* $\theta=0$.—The complete height distribution, v, is obtained by integrating v_1 with respect to θ, remembering that v_1^*, through x_1 and h_1, is a function of θ. To avoid confusion, we will let the values of h_1, α_1, p_1 for $\theta=0°$ be denoted by h_m, α_m, p_m, and put $x=(h-h_m)/H$. Thus they are related by the same equations (11) and (16).

Anticipating that the normalized distributions will not be strongly dependent upon the exact form of the polar diagram and on the other θ-dependent terms multiplying v_1^* in (13) and (14), we will restrict ourselves to consideration of (14) and neglect the variation of h_1 with θ. Thus we can put

$$\alpha_1=\alpha_m[\cos^{3/2}\theta\, S^2(\theta)]^{-1}=\alpha_m f^{-2}(u), \tag{20}$$

where $u=\tan\theta$, $f(u)=\cos^{3/4}\theta S(\theta)$ and α_m is the minimum detectable line density at range $h_m/\cos\chi$ in the direction of the principal maximum of the aerial beam (in the echo plane). Hence v is proportional to

$$\int_{-\infty}^{\infty} f^{2(s-1)}(u)\, v_1^* \, du.$$

Now $$x_1=-\ln(p/p_1)=-\ln(p/p_m)-\ln(p_m/p_1)=x-\tfrac{1}{3}\ln(\alpha_m/\alpha_1).$$

Therefore
$$x_1=x-\tfrac{2}{3}\ln f(u), \tag{21}$$

and
$$v(x)\propto\int_{-\infty}^{\infty}\left[\frac{e^x}{2f^{-1}(u)e^{3x/2}+1}\right]^{3(s-1)} du. \tag{22}$$

Mean height

The mean height is given by

$$\bar{x}=(\bar{h}-h_m)/H=\frac{\iint x f^{2(s-1)}(u) v_1^* \, du\, dx_1}{\iint f^{2(s-1)}(u) v_1^* \, du\, dx_1}, \tag{23}$$

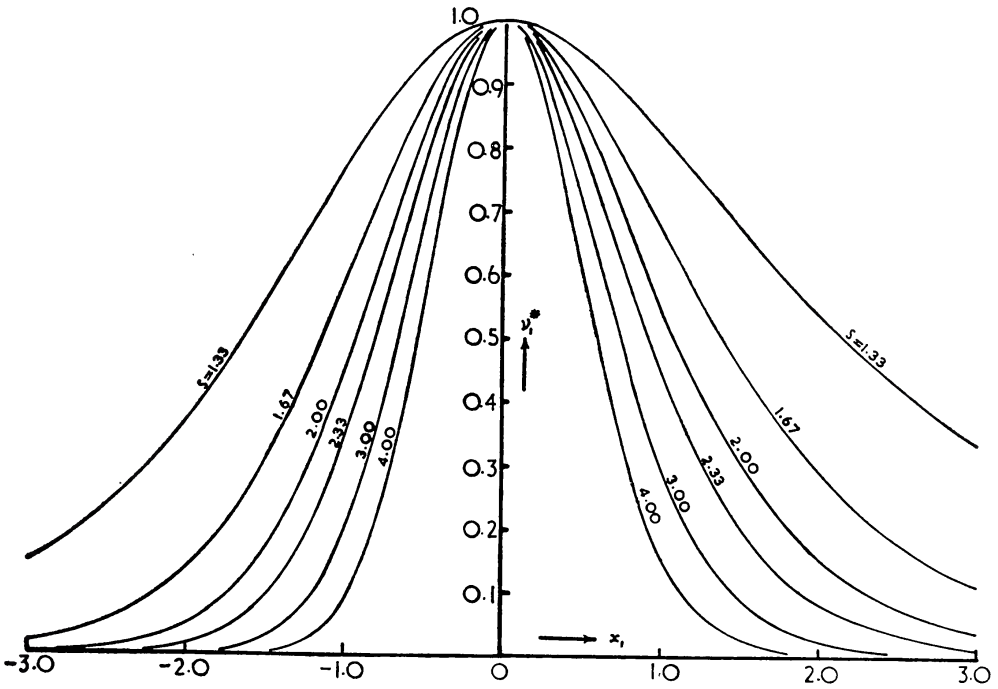

FIG. 2.—*Normalized distribution in height, v_1^*, of echoes observed in the sector $\theta-(\theta+d\theta)$ of the echo plane.* $x_1=(h-h_1)/H$.

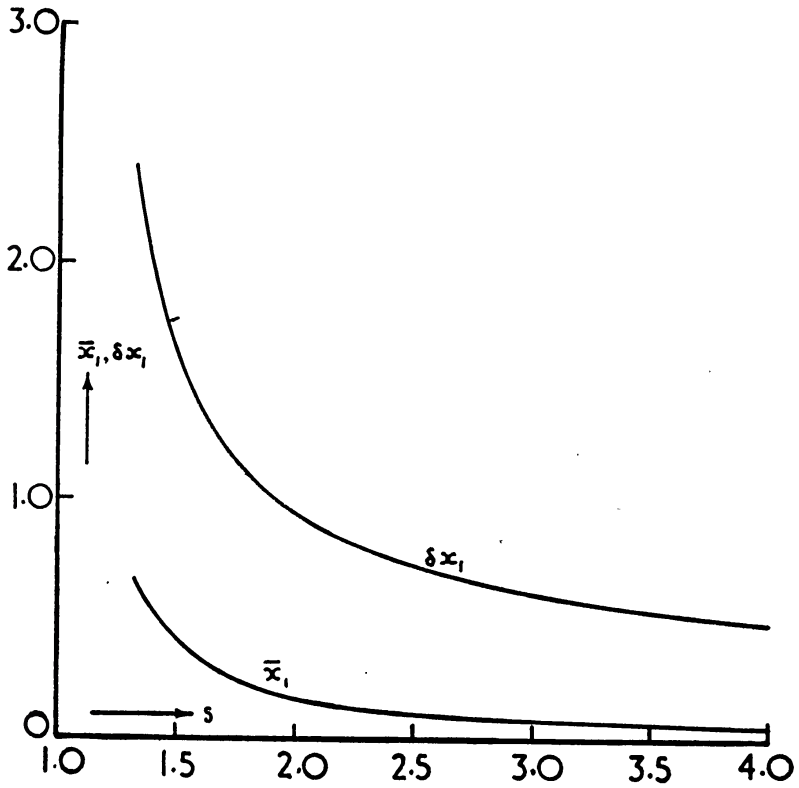

FIG. 3.—*Parameters of the distribution v_1^* as a function of s.*

the integrals being taken for both u and x between $-\infty$ and $+\infty$. Substituting (21) in (23) and remembering that

$$\int_{-\infty}^{\infty} x_1 \nu_1^* \, dx_1 \quad \text{and} \quad \int_{-\infty}^{\infty} \nu_1^* dx_1$$

are independent of θ, we have

$$\bar{x} - \bar{x}_1 = \tfrac{2}{3} \frac{\int_{-\infty}^{\infty} f^{2(s-1)}(u) \ln f(u) \, du}{\int_{-\infty}^{\infty} f^{2(s-1)}(u) \, du}. \tag{24}$$

R.m.s. height deviation from the mean

The r.m.s. deviation of x from $\bar{x}$, denoted by δx, is obtained from the elementary height distribution, ν_1^*, through

$$(\delta x)^2 = \frac{\iint (x-\bar{x})^2 f^{2(s-1)}(u) \nu_1^* \, du \, dx_1}{\iint f^{2(s-1)}(u) \nu_1^* \, du \, dx_1}.$$

Using the previous expansion (21) for x_1, we find

$$(x-\bar{x})^2 = (x_1-\bar{x}_1)^2 - 2(x_1-\bar{x}_1)(\bar{x}-\bar{x}_1) + (\bar{x}-\bar{x}_1)^2 + \tfrac{4}{3}(x_1-\bar{x}) \ln f(u) + \tfrac{4}{9} \ln^2 f(u),$$

leading to

$$(\delta x)^2 = (\delta x_1)^2 - (\bar{x}-\bar{x}_1)^2 + \tfrac{4}{9} \frac{\int_{-\infty}^{\infty} f^{2(s-1)}(u) \ln^2 f(u) \, du}{\int_{-\infty}^{\infty} f^{2(s-1)}(u) \, du}. \tag{25}$$

The value of (24) and (25) is that they enable the mean height and the r.m.s. height deviation to be evaluated in terms of the corresponding quantities for the elementary distribution ν_1^*, eliminating the necessity for evaluating ν^* explicitly.

Simple physical considerations show that the main effect of the polar diagram on the height distribution derives from the behaviour of $f(u)$ in the vicinity of $u = 0$. For this reason, the parameters of the height distribution have been determined for the following forms of $f(u)$:

(a) $(1+c^2u^2)^{-1}$ (b) $\exp(-c^2u^2)$ (c) $\cos^2 cu$ for $-\pi/2 < cu < \pi/2$ and zero otherwise.

All vary as $(1-c^2u^2)$ for small u but approach zero at different rates as $u \to \infty$. $\bar{x}$ and δx have also been evaluated numerically for $S(\theta) = \cos(\pi/2 \sin\theta)$, which corresponds approximately to the case of a horizontal half-wave dipole spaced $\leqslant \lambda/4$ above a reflecting ground plane. Almost any actual polar diagram will lead to a function $f(u)$ between the limits of (a) and (c). For example, the polar diagrams derived from (a), (b) and (c) for $c^2 = 1{\cdot}61$ are given in Fig. 4 (*a*), with $\cos(\pi/2 \sin\theta)$ (which has the same form near $\theta = 0$) for comparison (curve (*d*)). The case of $c^2 \gg 1$, when we can put $\theta \simeq \sin\theta \simeq \tan\theta$, is given in Fig. 4 (*b*) together with the polar diagram $[\sin(c\sqrt{6}\theta)]/(c\sqrt{6}\,\theta)$ for comparison (curve (*d*)).

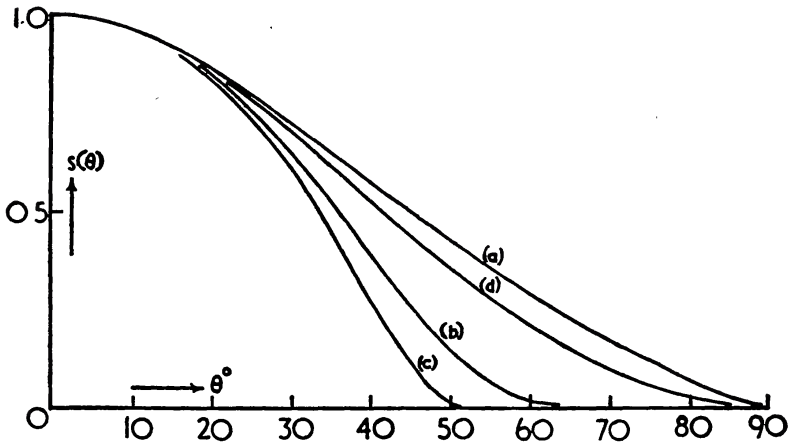

FIG. 4 (*a*).—*Aerial polar diagram, $S(\theta)$, in the echo plane.*
(*a*) $f(u)=(1+1\cdot61u^2)^{-1}$, (*b*) $f(u)=\exp(-1\cdot61u^2)$, (*c*) $f(u)=\cos^2(1\cdot27u)$, (*d*) $S(\theta)=\cos(\pi/2\sin\theta)$.

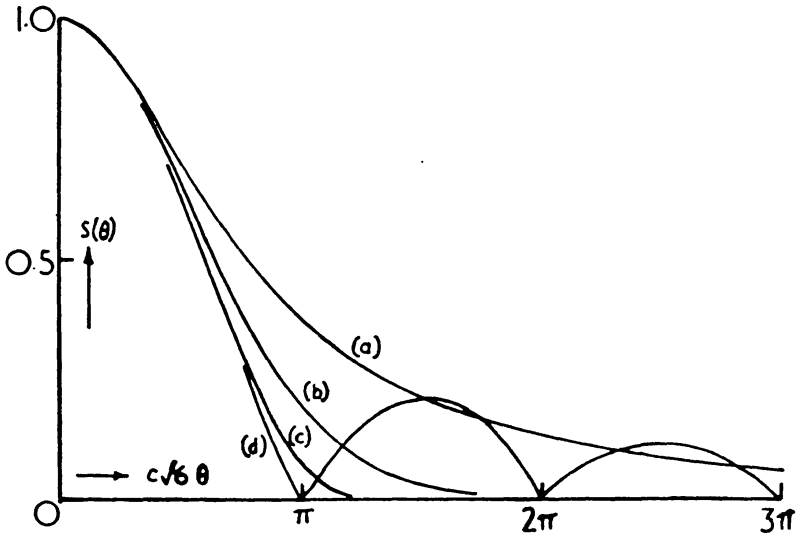

FIG. 4 (*b*).—*Aerial polar diagram, $S(\theta)$, in the echo plane for a beam sufficiently narrow that* $\theta \simeq \sin\theta \simeq \tan\theta$.
(*a*) $f(u)=(1+c^2u^2)^{-1}$, (*b*) $f(u)=\exp(-c^2u^2)$, (*c*) $f(u)=\cos^2(cu)$, (*d*) $S(\theta)=[\sin(c\sqrt{6\theta})]/(c\sqrt{6\theta})$.

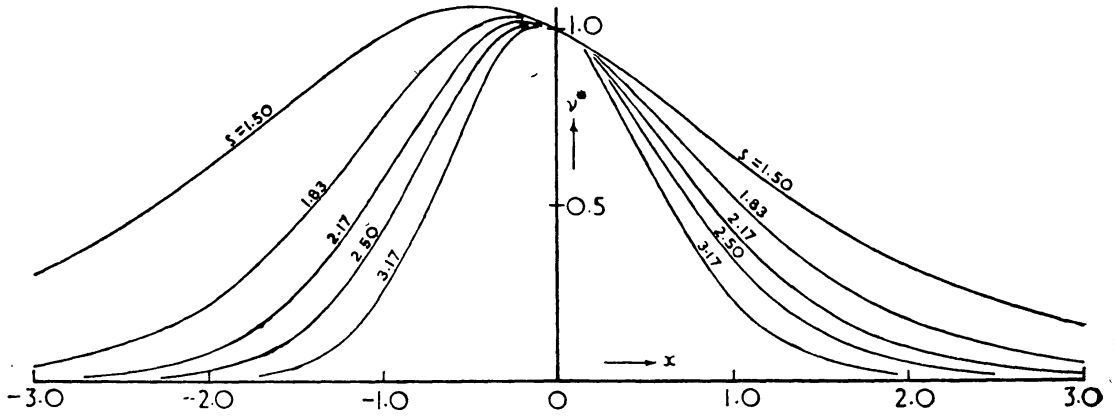

FIG. 5.—*Height distribution, v^*, as a function of x for an aerial polar diagram (in the echo plane) represented by* $f(u)=(1+c^2u^2)^{-1}$. $x=(h-h_m)/H$.

Case (a) $f(u)=(1+c^2u^2)^{-1}$

The integrals which we require for the evaluation of $\bar{x}$ and δx become, using the substitutions $cu=\tan v$, $q=4s-6$,

$$\int_{-\infty}^{\infty} f^{2(s-1)}(u)\,du=\frac{2}{c}\int_0^{\pi/2}\cos^q v\,dv, \tag{26}$$

$$\int_{-\infty}^{\infty} f^{2(s-1)}(u)\ln f(u)\,du=\frac{4}{c}\int_0^{\pi/2}\cos^q v\ln(\cos v)\,dv, \tag{27}$$

$$\int_{-\infty}^{\infty} f^{2(s-1)}(u)\ln^2 f(u)\,du=\frac{8}{c}\int_0^{\pi/2}\cos^q v\ln^2(\cos v)\,dv. \tag{28}$$

For integral values of q, (26) is easily evaluated, and for (27) and (28) we obtain the recurrence formulae:

$$q\int_0^{\pi/2}\cos^q v\ln(\cos v)\,dv=(q-1)\int_0^{\pi/2}\cos^{q-2}v\ln(\cos v)\,dv+\int_0^{\pi/2}\cos^{q-2}v\,dv - \int_0^{\pi/2}\cos^q v\,dv, \tag{29}$$

$$q\int_0^{\pi/2}\cos^q v\ln^2(\cos v)\,dv=(q-1)\int_0^{\pi/2}\cos^{q-2}v\ln^2(\cos v)\,dv +2\int_0^{\pi/2}\cos^{q-2}v\ln(\cos v)\,dv-2\int_0^{\pi/2}\cos^q v\ln(\cos v)\,dv. \tag{30}$$

These integrals have been evaluated numerically for $q=0$, 1.

From (22) the height frequency distribution, normalized to unity at $x=0$, is found to be

$$v^*(x)=e^{-x/4}\left[\frac{3e^x}{2e^{3x/2}+1}\right]^{3s-7/2}, \tag{31}$$

which is plotted in Fig. 5 for various values of s.

Case (b) $f(u)=\exp(-c^2u^2)$

Putting $cu=v$, we have

$$\int_{-\infty}^{\infty} f^{2(s-1)}(u)\,du=\frac{2}{c}\int_0^{\infty} e^{-2(s-1)v^2}\,dv,$$

$$\int_{-\infty}^{\infty} f^{2(s-1)}(u)\ln f(u)\,du=-\frac{1}{2c(s-1)}\int_0^{\infty} e^{-2(s-1)\,v^2}\,dv,$$

$$\int_{-\infty}^{\infty} f^{2(s-1)}(u)\ln^2 f(u)\,du=\frac{3}{8c(s-1)^2}\int_0^{\infty} e^{-2(s-1)\,v^2}\,dv,$$

hence

$$\bar{x}=\bar{x}_1-\frac{1}{6(s-1)}, \tag{32}$$

$$(\delta x)^2=(\delta x_1)^2+\frac{1}{18(s-1)^2}. \tag{33}$$

The function v^* has not been determined for this case.

Case (c) $f(u)=\cos^2 cu$

Putting $cu=v$, $q=4(s-1)$, we obtain the same equations as for Case (a), namely (26), (27), (28).

Equation (22) is integrable for integral values of $3s-7/2$, giving

$$v^*(x) \propto e^{(3s-7/2)x}\left[\sin^{-1}y - y\sqrt{(1-y^2)}\sum_{n=1}^{3s-7/2}\left(1+\frac{2.4.6....2n}{3.5.7....(2n+1)}y^{2n}\right)\right], \quad (34)$$

where $y=2e^{3x/2}+1$, which is given in Fig. 6 for various values of s.

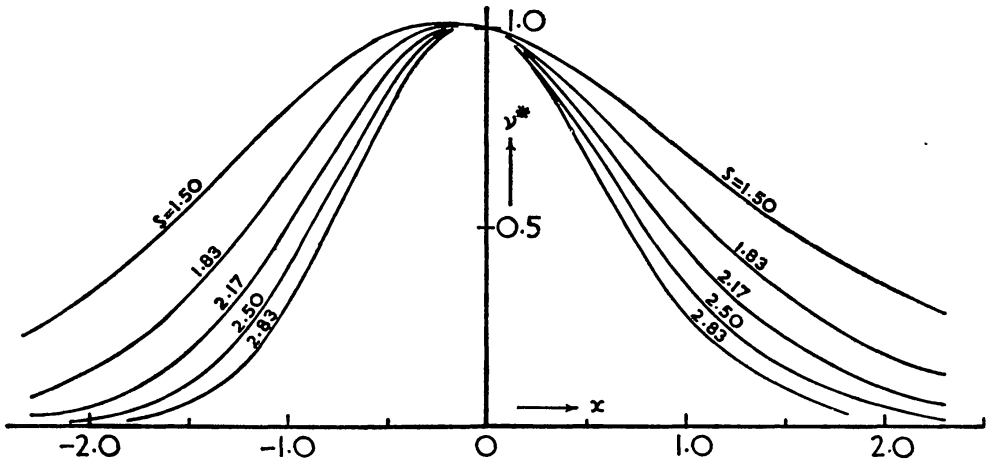

FIG. 6.—*Height distribution, v^*, as a function of x for an aerial polar diagram (in the echo plane) represented by $f(u)=\cos^2 cu$. $x=(h-h_m)/H$.*

Figs. 7 (*a*) and 7 (*b*) show $\bar{x}$ and δx as a function of s for the cases considered above. It will be noted that, as anticipated, the height distribution is remarkably insensitive to the exact form of $f(u)$, and hence of the polar diagram. For the same reason, the complete height distribution for v_1 given by (13) will not be significantly different from those derived above.

4.4. *Complete height distribution, polar diagram symmetrical about $\theta=\theta_0$.*—In this section we will let h_m, α_m, etc., be the values of h_1, α_1, etc., at $\theta=\theta_0$, i.e. as before, the quantities appropriate to the direction of the principal maximum of the aerial beam in the echo plane. Since the foregoing has shown that the height distribution is not critically dependent on the exact form of the function of θ multiplying v_1^* in (13) and (14), we will restrict the discussion to the case of an aerial beam sufficiently narrow that we may write $\alpha_1 \simeq \alpha_m S^{-2}(\theta')$, $\cos\theta \simeq \cos\theta_0$, where $\theta'=\theta-\theta_0$. Hence, from (14),

$$v_1 \simeq \frac{b}{(s-1)}\left(\frac{4k_1\cos\chi}{9\alpha_1}\right)^{s-1}\frac{h_1}{\sin^2\phi}v_1^*, \quad (35)$$

where $\sin\phi=\cos\theta_0\sin\chi$, i.e. ϕ is the elevation of the principal maximum of the beam in the echo plane. Putting $\tan\theta'=u$, $f(u)\simeq S(\theta')$, v^* is given by (22), i.e. is identical with the previous case, and the characteristics of the height distributions for the various $f(u)$ are given by Figs. 5, 6 and 7.

As the elevation ϕ tends to zero, v_1 may be found from (13), which, provided θ_0 does not approach 90°, leads to a result identical with (35) except that the factor $h_1/\sin^2\phi$ is replaced by R_e.

4.5. *Equipment sensitivity such that $\alpha_m \gg 10^{12}\,\mathrm{cm}^{-1}$.*—We will deal briefly with this case for which only the long-duration echoes are observed.

We proceed as before, except that instead of (6) we find $\alpha_p^{1/4}$ to be proportional to $R^{3/2}S^{-2}(\theta)$ (1). Thus $\alpha_1=\alpha_m[\cos^6\theta\, S^8(\theta)]^{-1}$. Equations (13) and (14) remain

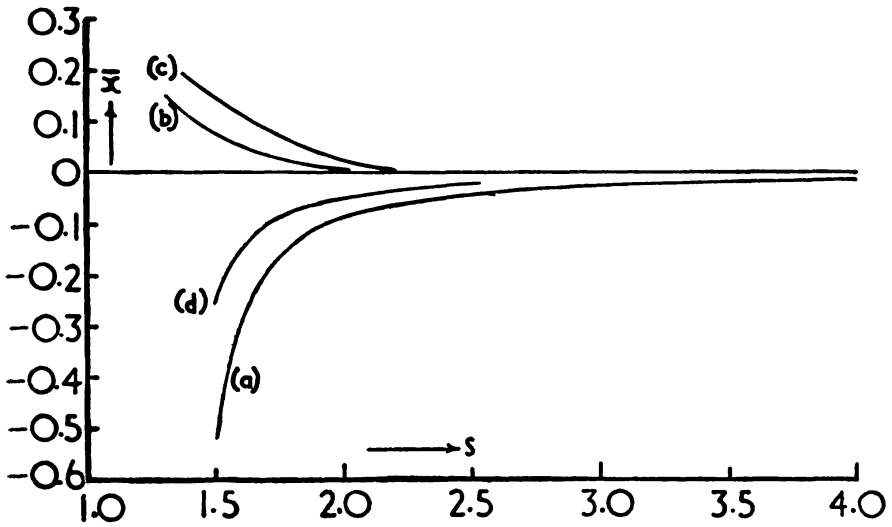

(*a*)

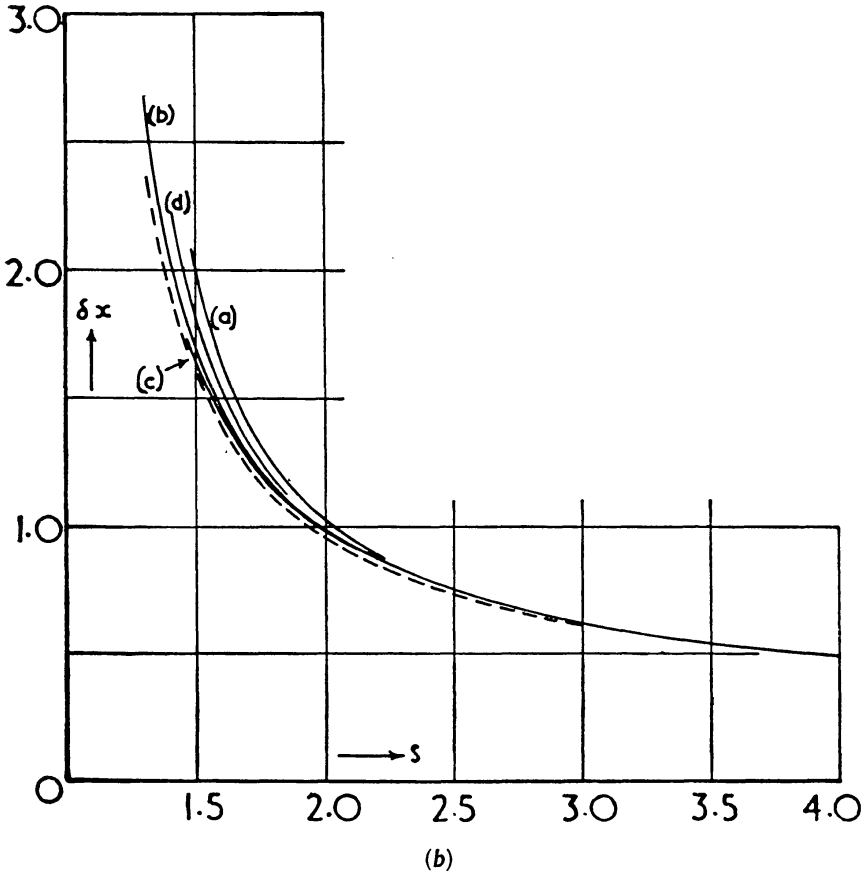

(*b*)

FIGS. 7 (*a*) *and* (*b*).—*Parameters of the height distribution as a function of s for an aerial polar diagram (in the echo plane) represented by:*

(*a*) $f(u)=(1+c^2u^2)^{-1}$, (*b*) $f(u)=\exp(-c^2u^2)$, (*c*) $f(u)=\cos^2 cu$, (*d*) $S(\theta)=\cos[(\pi/2)\sin\theta]$. *The broken curve in Fig. 7 (b) gives the r.m.s deviation,* δx_1, *for the elementary distribution* v_1*.

valid, as does the remainder of the analysis except that $f^4(u)$ replaces $f(u)$ throughout. For $f(u)=(1+c^2u^2)^{-1}$ and $f(u)=\cos^2 cu$ both $\bar{x}$ and δx are more nearly equal to the values obtained for $f(u)=\exp(-c^2u^2)$, which remain unchanged. Fig. 8 gives $\bar{x}$ vs. s for the three cases; the values of δx are not given, since they do not differ significantly.

For α_m in the transition region (i.e. echoes distributed more or less evenly between the two types) simple physical considerations show that the previous results are still satisfactory, with the values of $\bar{x}$ and δx slightly nearer to $\bar{x}_1$ and δx_1.

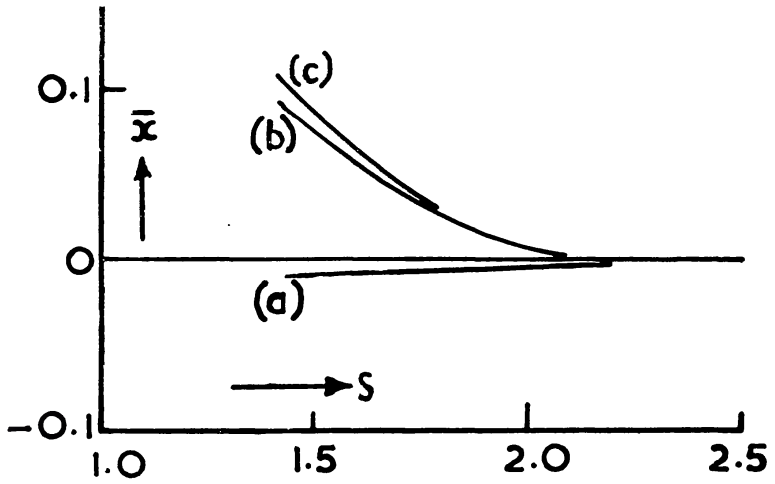

FIG. 8.—$\bar{x}=(\bar{h}-h_m)/H$ *as a function of s for an equipment of such low sensitivity that* $\alpha_m \gg 10^{12}$ *cm*$^{-1}$.
(*a*) $f(u)=(1+c^2u^2)^{-1}$, (*b*) $f(u)=\exp(-c^2u^2)$, (*c*) $f(u)=\cos^2 cu$.

5. *Discussion.*—The above theory makes possible the interpretation of the meteor height distribution observed on a radio-echo equipment during the activity of a major meteor stream.

The width of the height distribution, expressed as the r.m.s. height deviation from the mean, depends on the atmospheric scale height, the mass distribution of the incident meteors, and only very slightly on the form of the aerial polar diagram. It will be shown in a later paper that the exponent s in the mass law may be obtained with fair precision from the echo amplitude and duration distributions; thus the scale height may be determined.

The mean height is close to the height h_m at which the pressure, p_m, is given by

$$p_m = k_2[9\alpha_m \cos^2\chi/4k_1]^{1/3}. \qquad (36)$$

It depends strongly on the meteor velocity which enters (36) through k_2 (which is proportional to v^{-2}) and possibly through the probability of ionization, β, contained in k_1. It is also dependent upon α_m, the minimum electron line density detectable at range $h_m/\sin\phi$ in the direction of the principal maximum of the aerial beam in the echo plane; α_m may be evaluated from the equipment parameters or derived from the amplitudes and durations of the long-duration echoes. Thus p_m can be obtained in terms of the physical properties of the meteors (latent heat, density, velocity), the radiant zenith angle χ, the heat transfer coefficient and the probability of ionization. The latter need not be known with great accuracy, since it enters (36) as the cube root.

The zenith angle χ has been treated throughout as constant. It is thus desirable that the height distribution be measured over a selected time interval

during the passage of the radiant across the sky, sufficiently short that the variation of χ may be neglected. This is not a severe restriction, since p_m is proportional to $\cos^{2/3}\chi$. As an example, if χ varies from 35° to 55°, the mean height changes by about 0·25 scale heights and if observations were extended over this range of χ, the width of the height distribution for $s\sim 2$, would not be more than some three per cent greater than the theoretical values derived above. The assumption of a well-defined radiant point merely requires the spread in meteor radiants to be small compared with the aerial beam width.

We have represented the polar diagram of the aerial beam in the echo plane by $S(\theta)$. In the case of an equipment using separate transmitting and receiving aerials with polar diagrams $S_T(\theta)$, $S_R(\theta)$ and gains G_T and G_R respectively, we simply write $S^2(\theta) = S_T(\theta)\, S_R(\theta)$, $G^2 = G_T\, G_R$.

University of Manchester,
Jodrell Bank Experimental Station,
Lower Withington,
Cheshire:
1953 *July*.

References

(1) Kaiser, T. R. and Closs, R. L., *Phil. Mag.*, **43**, 1, 1952.
(2) Closs, R. L., Clegg, J. A. and Kaiser, T. R., *Phil. Mag.*, **44**, 313, 1953.
(3) Clegg, J. A. and Davidson, I. A., *Phil. Mag.*, **41**, 77, 1950.
(4) Kaiser, T. R. and Greenhow, J. S., *Proc. Phys. Soc.* B, **66**, 150, 1953.
(5) Herlofson, N., *Phys. Soc. Rep. Prog. Phys.*, **11**, 444, 1948.
(6) Whipple, F. L., *Advances in Geophysics*, I, p. 119, Academic Press Inc., New York, 1952.
(7) Watson, F., *Harv. Ann.*, **105**, 623, 1937.
(8) Watson, F., *Between the Planets*, Blakiston, 1941.
(9) Williams, J. D., *A.J.*, **92**, 424, 1940.
(10) Greenhow, J. S., *Proc. Phys. Soc.* B, **65**, 169, 1952.